Proc. 6th Asian Conference on Computer Vision (ACCV 2004), January 2004, Jeju, Korea, Vol. 1, pp. 1–6.

STABILIZING THE FOCAL LENGTH COMPUTATION FOR 3-D RECONSTRUCTION FROM TWO UNCALIBRATED VIEWS

Atsutada Nakatsuji[*]*, Shigeo Takahashi*[†]*, Yasuyuki Sugaya*[†]*, and Kenichi Kanatani*[†]

[*]System Solutions Division II, NEC Engineering, Ltd., Fuchu-shi, Tokyo 183-8502 Japan
[†] Department of Information Technology, Okayama University, Okayama 700-8530 Japan
{nakatuji,shigeo,sugaya,kanatani}@suri.it.okayama-u.ac.jp

ABSTRACT

In order to reconstruct 3-D shape from two uncalibrated views, one needs to resolve two problems: (i) the computed focal lengths can be imaginary; (ii) the computation fails for fixated images. We present a remedy for these by subsampling feature points and fixing the focal length. We first summarize theoretical backgrounds and then do simulations, which reveal a rather surprising fact that when the focal length is actually fixed, not using that knowledge yields better results for non-fixated images. We propose a hybrid method switching the computation by judging whether or not the images are fixated. Doing simulations and real image experiments, we demonstrate the effectiveness of our method.

1. INTRODUCTION

Many techniques have been proposed for reconstructing 3-D shape from images [6]. They are classified into two types: using separate images and using a continuous video stream. Among the former, the two-view method using two uncalibrated images [5, 13] is the simplest. Using three or more images may improve the accuracy, but a large amount of computation is necessary for matching multiple images and estimating the camera positions and their internal parameters for all the frames [16]. In contrast, the two-view method merely requires one to match feature points between the two images and compute the fundamental matrix. Today, effective algorithms are available for robustly matching two images [14, 18] and for accurately computing the fundamental matrix [3, 10, 15], making the two-view method more and more practical for real applications.

However, this method has a serious drawback: since all the computations are based on the feature point matches over two images, the result is very sensitive to the quality of the matches. In particular, the focal lengths for the two images are often computed to be imaginary [5] due to matching inaccuracies; wrong points may be matched, or the matched points may not exactly correspond to identical points in the scene.

On top of that, the computation fails if the two images are such that a point in the scene is fixated at their principal points [2, 12]; we call such an image pair *fixated images*. In order to do 3-D reconstruction, therefore, one must avert the camera from the object in a different way for each image. This is a big obstacle in practice, since for humans it is most natural to take images of something by fixating it.

This paper analyzes these problems in detail and presents a remedy. First, we avoid imaginary focal lengths by subsampling feature points. To cope with fixated images, we fix the focal length for the two images. It is known that 3-D reconstruction is possible even from fixated images if the two focal lengths are the same [2, 12]. This is not a serious constraint, since the focus and zooming are usually fixed in the course of taking pictures for 3-D reconstruction.

However, we reveal a rather surprising fact in this paper: when the focal length is actually fixed, *not using that knowledge yields better results if the images are not fixated*. Exploiting this fact, we propose a hybrid method switching the computation by judging whether or not the images are fixated. Doing simulations and real image experiments, we demonstrate the effectiveness of our method.

2. GEOMETRY OF FIXATED IMAGES

We first summarize our assumptions, terminologies, and notations. We assume that the camera skew angle is 0° and the aspect ratio is 1. Most digital cameras today seem to satisfy these conditions. If not, appropriate geometric correction is not difficult.

Heyden and Åström [7] showed that if such a camera is used, the 3-D reconstruction is possible without knowing the focal length and the principal point location, but generally we need three or more images. Hartley [4] showed that two images are sufficient if the principal point is given. We assume that it is known (typically at the center of the image frame) and take it as the image coordinate origin. However, the focal length is assumed to be unknown.

If a point (x, y) in the first image corresponds to a point (x', y') in the second, the following *epipolar equation* should be satisfied [6]:

$$(\boldsymbol{x}, \boldsymbol{F}\boldsymbol{x}') = 0. \tag{1}$$

Throughout this paper, we denote the inner product of vectors $\boldsymbol{a}$ and $\boldsymbol{b}$ by $(\boldsymbol{a}, \boldsymbol{b})$. We define 3-D vectors

$$\boldsymbol{x} = \begin{pmatrix} x/f_0 \\ y/f_0 \\ 1 \end{pmatrix}, \quad \boldsymbol{x}' = \begin{pmatrix} x'/f_0 \\ y'/f_0 \\ 1 \end{pmatrix}, \tag{2}$$

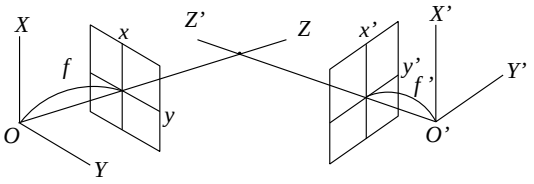

Fig. 1. Two images are fixated if the optical axes intersect.

where f_0 (the unit is pixels) is a scale factor[1] for stabilizing numerical computation. The matrix $\boldsymbol{F}$ in eq. (1) is of rank 2 and called the *fundamental matrix* [6].

We say that two images are *fixated* if the optical axes of the cameras that took these images intersect in the scene (Fig. 1). It follows that the origin of one image corresponds to the origin of the other. In the vector representation of eqs. (2), the origin is represented by $\boldsymbol{k} = (0, 0, 1)^\top$. So, the condition for fixation is

$$(\boldsymbol{k}, \boldsymbol{F}\boldsymbol{k}) = 0, \tag{3}$$

or equivalently $F_{33} = 0$.

3. VARIABLE FOCAL LENGTH METHOD

We next summarize the method for computing the focal lengths f and f' of the two cameras from the fundamental matrix $\boldsymbol{F}$ [1, 12]. First, we change the variables as follows:

$$\xi = \left(\frac{f_0}{f}\right)^2 - 1, \qquad \eta = \left(\frac{f_0}{f'}\right)^2 - 1. \tag{4}$$

Define the following fourth-order polynomial $K(\xi, \eta)$:

$$\begin{aligned} K(\xi,\eta) = {} & (\boldsymbol{k}, \boldsymbol{F}\boldsymbol{k})^4\xi^2\eta^2 + 2(\boldsymbol{k}, \boldsymbol{F}\boldsymbol{k})^2\|\boldsymbol{F}^\top\boldsymbol{k}\|^2\xi^2\eta \\ & + 2(\boldsymbol{k}, \boldsymbol{F}\boldsymbol{k})^2\|\boldsymbol{F}\boldsymbol{k}\|^2\xi\eta^2 + \|\boldsymbol{F}^\top\boldsymbol{k}\|^4\xi^2 \\ & + \|\boldsymbol{F}\boldsymbol{k}\|^4\eta^2 + 4(\boldsymbol{k}, \boldsymbol{F}\boldsymbol{k})(\boldsymbol{k}, \boldsymbol{F}\boldsymbol{F}^\top\boldsymbol{F}\boldsymbol{k})\xi\eta \\ & + 2\|\boldsymbol{F}\boldsymbol{F}^\top\boldsymbol{k}\|^2\xi + 2\|\boldsymbol{F}^\top\boldsymbol{F}\boldsymbol{k}\|^2\eta + \|\boldsymbol{F}\boldsymbol{F}^\top\|^2 \\ & - \frac{1}{2}\Big((\boldsymbol{k}, \boldsymbol{F}\boldsymbol{k})^2\xi\eta + \|\boldsymbol{F}^\top\boldsymbol{k}\|^2\xi \\ & + \|\boldsymbol{F}\boldsymbol{k}\|^2\eta + \|\boldsymbol{F}\|^2\Big)^2. \end{aligned} \tag{5}$$

The unknowns ξ and η are determined from the following condition [12]:

$$K = \frac{\partial K}{\partial \xi} = \frac{\partial K}{\partial \eta} = 0. \tag{6}$$

This appears to be overspecification, providing three equations for two unknowns. Under close scrutiny, however, it turns out that the three equations are algebraically dependent, only two among them being independent [12]. Geometrically, the function $K(\xi, \eta)$ defines a locally nonnegative concave surface that is tangent to the $\xi\eta$-plane with minimum 0 (Fig. 2).

[1]We used the value $f = 600$ in our experiment, but no practical difference should result by letting $f_0 = 1$.

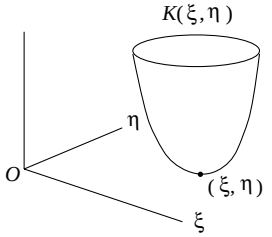

Fig. 2. The focal lengths f and f' are determined by the tangent point of the surface $K(\xi, \eta)$ to the $\xi\eta$-plane, at which $K(\xi, \eta)$ takes its minimum 0.

Since $K(\xi, \eta)$ is a fourth degree polynomial, its minimum can be easily computed by Newton iterations. Also, many analytical formulae are known for the solution [12]. Among them, the simplest is the following formula of Kanatani and Matsunaga [12] obtained by modifying Bougnoux's formula [1]:

$$\begin{aligned} \xi &= \frac{\|\boldsymbol{F}\boldsymbol{k}\|^2 - (\boldsymbol{k}, \boldsymbol{F}\boldsymbol{F}^\top\boldsymbol{F}\boldsymbol{k})\|\boldsymbol{e}' \times \boldsymbol{k}\|^2/(\boldsymbol{k}, \boldsymbol{F}\boldsymbol{k})}{\|\boldsymbol{e}' \times \boldsymbol{k}\|^2\|\boldsymbol{F}^\top\boldsymbol{k}\|^2 - (\boldsymbol{k}, \boldsymbol{F}\boldsymbol{k})^2}, \\ \eta &= \frac{\|\boldsymbol{F}^\top\boldsymbol{k}\|^2 - (\boldsymbol{k}, \boldsymbol{F}\boldsymbol{F}^\top\boldsymbol{F}\boldsymbol{k})\|\boldsymbol{e} \times \boldsymbol{k}\|^2/(\boldsymbol{k}, \boldsymbol{F}\boldsymbol{k})}{\|\boldsymbol{e} \times \boldsymbol{k}\|^2\|\boldsymbol{F}\boldsymbol{k}\|^2 - (\boldsymbol{k}, \boldsymbol{F}\boldsymbol{k})^2}. \end{aligned} \tag{7}$$

Here, $\boldsymbol{e}$ and $\boldsymbol{e}'$ are, respectively, the unit eigenvectors of $\boldsymbol{F}\boldsymbol{F}^\top$ and $\boldsymbol{F}^\top\boldsymbol{F}$ for eigenvalue[2] 0; they represent the *epipoles* [6], pointing from the respective centers of projection to the centers of projection of the other images.

From eqs. (7), it is immediately seen that the computation fails for fixated images, for which $(\boldsymbol{k}, \boldsymbol{F}\boldsymbol{k})$ vanishes, causing zero division. Otherwise, the focal lengths f and f' are given from eqs. (4) as follows:

$$f = \frac{f_0}{\sqrt{1+\xi}}, \qquad f' = \frac{f_0}{\sqrt{1+\eta}}. \tag{8}$$

However, if the computed fundamental matrix $\boldsymbol{F}$ is not accurate enough, the inside of one or both of the square roots can be negative, resulting in imaginary focal lengths [5].

4. FIXED FOCAL LENGTH METHOD

We now describe our scheme for computing the focal lengths f and f' by using the knowledge that they are equal. If we let $\xi = \eta$ in eq. (5), we obtain the following fourth-degree polynomial $K(\xi)$:

$$K(\xi) = a_1\xi^4 + a_2\xi^3 + a_3\xi^2 + a_4\xi + a_5, \tag{9}$$

$$\begin{aligned} a_1 &= \frac{1}{2}(\boldsymbol{k}, \boldsymbol{F}\boldsymbol{k})^4, \\ a_2 &= (\boldsymbol{k}, \boldsymbol{F}\boldsymbol{k})^2(\|\boldsymbol{F}^\top\boldsymbol{k}\|^2 + \|\boldsymbol{F}\boldsymbol{k}\|^2), \\ a_3 &= \frac{1}{2}(\|\boldsymbol{F}^\top\boldsymbol{k}\|^2 - \|\boldsymbol{F}\boldsymbol{k}\|^2)^2 \end{aligned}$$

[2]Even in the presence of noise, the fundamental matrix $\boldsymbol{F}$ is computed to be $\det \boldsymbol{F} = 0$, so $\boldsymbol{F}\boldsymbol{F}^\top$ and $\boldsymbol{F}^\top\boldsymbol{F}$ both have eigenvalue 0.

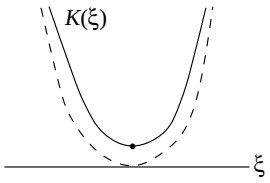

Fig. 3. The focal length can be determined by the position at which the curve $K(\xi)$ takes its minimum 0. However, the minimum is generally positive.

$$
\begin{aligned}
&+(\boldsymbol{k}, \boldsymbol{F}\boldsymbol{k})(4(\boldsymbol{k}, \boldsymbol{F}\boldsymbol{F}^\top\boldsymbol{F}\boldsymbol{k}) - (\boldsymbol{k}, \boldsymbol{F}\boldsymbol{k})\|\boldsymbol{F}\|^2),\\
a_4 &= 2(\|\boldsymbol{F}\boldsymbol{F}^\top\boldsymbol{k}\|^2 + \|\boldsymbol{F}^\top\boldsymbol{F}\boldsymbol{k}\|^2)\\
&\quad -(\|\boldsymbol{F}^\top\boldsymbol{k}\|^2 + \|\boldsymbol{F}\boldsymbol{k}\|^2)\|\boldsymbol{F}\|^2,\\
a_5 &= \|\boldsymbol{F}\boldsymbol{F}^\top\|^2 - \frac{1}{2}\|\boldsymbol{F}\|^4. \qquad (10)
\end{aligned}
$$

Eq. (6) reduces to

$$K(\xi) = K'(\xi) = 0. \qquad (11)$$

The solution is analytically obtained as follows [12]:

- If $a_1 \neq 0$,
  - if $3a_2^2 - 8a_1a_3 \neq 0$, compute the two solutions of the quadratic equation

$$
\begin{aligned}
&(3a_2^2 - 8a_1a_3)x^2 + 2(a_2a_3 - 6a_1a_4)x\\
&\qquad +(a_2a_4 - 16a_1a_5) = 0. \qquad (12)
\end{aligned}
$$

    Let ξ be the one for which $|K(x)|$ is smaller;
  - if $3a_2^2 - 8a_1a_3 = 0$, let

$$\xi = -\frac{a_2a_4 - 16a_1a_5}{2(a_2a_3 - 6a_1a_4)}. \qquad (13)$$

- If $a_1 = 0$ and $a_2 \neq 0$, let

$$\xi = -\frac{a_3a_4 - 9a_2a_5}{2(a_3^2 - 3a_2a_4)}. \qquad (14)$$

- If $a_1 = a_2 = 0$ and $a_3 \neq 0$, let

$$\xi = -\frac{a_4}{2a_3}. \qquad (15)$$

- If $a_1 = a_2 = a_3 = 0$, no solution exists.

However, this analysis is based on the assumption that the fundamental matrix $\boldsymbol{F}$ is exact. Eq. (11) gives two constraints on one variable ξ. If $\boldsymbol{F}$ is computed from noisy data, the two constraints are in general inconsistent.

Geometrically, eq. (11) states that the solution is given by the position on the ξ-axis at which the curve $K(\xi)$ takes its minimum 0. However, the minimum is in general positive (Fig. 3), because $K(\xi)$ is the cross section of the surface $K(\xi, \eta)$ in Fig. 2 with a plane perpendicular to the $\xi\eta$-plane passing through the line $\xi = \eta$. It follows that the minimum of $K(\xi)$ is 0 when and only when the minimum of $K(\xi, \eta)$ is on the line $\xi = \eta$. This condition is generally violated if $\boldsymbol{F}$ is not exact.

Ueshiba and Tomita [17] analytically obtained a unique solution by regarding the two principal points as extra unknowns, assuming that the images are fixated. However, the camera must be rotated around the optical axis for the solution to exist. Also, their method cannot be applied to non-fixated images.

In order to avoid this difficulty, we compute the value ξ at which the curve $K(\xi)$ takes its minimum, i.e., we solve $K'(\xi) = 0$. Since $K'(\xi)$ is a cubic polynomial, the solution can be analytically obtained in theory. However, the computation branches depending on whether $a_1 \sim a_3$ are zero or not, and there is no good way to set a suitable threshold for that judgment.

This is resolved by numerically computing the solution of $K'(\xi) = 0$ by Newton iterations in the form

$$\xi \leftarrow \xi - \frac{K'(\xi)}{K''(\xi)}. \qquad (16)$$

We use eq. (15) as the initial value. This numerical scheme completely avoids the zero/non-zero judgment of the coefficients; usually the solution is obtained after two or three iterations. From the computed ξ, the focal lengths f and f' are given by eqs. (8), namely,

$$f = f' = \frac{f_0}{\sqrt{1 + \xi}}. \qquad (17)$$

In this case, too, the solution can be imaginary.

5. VARIABLE VS. FIXED FOCAL LENGTHS

The focal lengths can be imaginary in the presence of noise whether we use the variable focal length method or the fixed focal length method. But which is better if the ground truth is $f = f'$? We examined this by simulation.

Fig. 4 shows two simulated images of a cylindrical grid surface. The image size is supposedly 600×800 pixels; the focal lengths are $\bar{f} = \bar{f}' = 1000$ (pixels). The center of

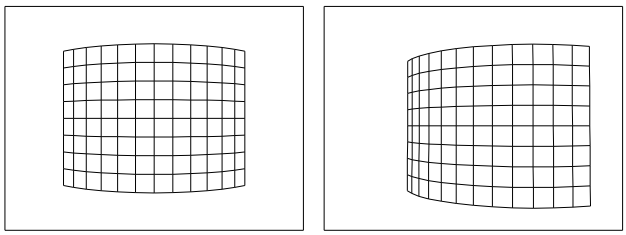

Fig. 4. Simulated images of a cylindrical grid surface (600×800 pixels). The focal lengths are $\bar{f} = \bar{f}' = 1000$ (pixels). The center of the second frame is displaced by d (= 20 for the images shown here) pixels from its fixated position.

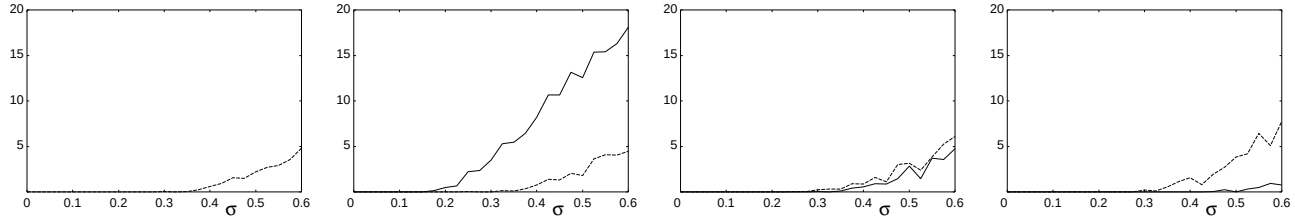

Fig. 5. The horizontal axis is for the noise standard deviation σ (pixels). The vertical axis shows the percentage of the occurrences of imaginary focal lengths. The solid and dashed lines are for the variable and fixed focal length methods, respectively. The value d (pixels) measures the deviation from fixation.

the second frame is displaced from its fixated position by d pixels, which we varied over $0 \leq d \leq 30$ (Fig. 4 shows the images for $d = 20$).

We added Gaussian noise of mean 0 and standard deviation σ (pixels) to the x and y coordinates of the 117 vertices independently. In order to simulate realistic situations, we randomly chose 10% of the vertices and increased the noise magnitude five times there. From these noisy vertices, we computed the fundamental matrix; we used an algorithm called *renormalization*[3] [10, 13], which is known to be statistically optimal [8].

Fig. 5 plots the percentage of the occurrences of imaginary focal lengths over 2000 trials for each σ. The solid and dashed lines are for the variable and fixed focal length methods, respectively. At $d = 0$ (fixated images), the values for the variable focal length method are not plotted, because they are out of the range; they are about 60% for all σ.

As d increases, the percentage for the variable focal length method drops, while it stays almost the same for the fixed focal length method. As a result, the relative order is reversed near $d = 20$.

6. ACCURACY OF THE FOCAL LENGTHS

In order to see the comparative accuracy of the focal lengths computed by the two methods, we need to avoid the occurrences of imaginary focal lengths.

To this end, Hartley and Silpa-Anan [5] used the knowledge about the approximate focal length and its minimum value: they optimized the fundamental matrix and the principal points so that the computed focal lengths are close to each other, close to their estimates, and close to their minimum values. The result depends on the estimates we use and the measure of closeness used in the objective function.

Here, we adopt subsampling of feature points. If the computed focal lengths are not both real, we randomly remove one pair of corresponding feature points and recompute the fundamental matrix. If we fail to obtain real focal lengths for $N/10$ consecutive repetitions (N is the number of correspondences), we randomly remove two pairs and do the same. If this fails, we go on removing more pairs until real focal lengths are obtained.

[3]The C++ source code is available at: http://www.img.tutkie.tut.ac.jp

Many other strategies can be conceivable. For example, we may prefer those feature points whose distances from their epipolar lines predicted by the fundamental matrix $\boldsymbol{F}$ in the preceding step are small. We tried such methods in many forms, but we were unable to find any method better than the above straightforward one.

We evaluated the accuracy of the computed focal lengths by the root-mean-square error

$$E = \sqrt{\frac{1}{2000}\sum_{a=1}^{1000}\Big((f_a - \bar{f})^2 + (f'_a - \bar{f}')^2\Big)} \qquad (18)$$

over 1000 trials, where f_a and f'_a are the computed values in the ath trial, and $\bar{f}$ and $\bar{f}'$ are their true values. We computed this for different σ and d, using the simulated images of Fig 4. Fig. 6 shows the results corresponding to Fig. 5.

From this, we see that the focal lengths computed by the variable focal length method from fixated images ($d = 0$) are meaningless, while the fixed focal length method can successfully compute fairly accurate values. However, the variable focal length method gradually gains in accuracy as d increases, while the fixed focal length method has almost the same accuracy. As a result, the relative accuracy is reversed around $d = 20$.

The low accuracy of the variable focal length method for a small d may be partly due to the numerical instability of computing eqs. (7) and partly due to the high percentage of imaginary focal lengths; subsampling of feature points generally degrades the accuracy.

7. HYBRID METHOD

From the above results, we can expect high accuracy if we use the fixed focal length method when the images are nearly fixated and the variable focal length method when they are not. Here, we adopt the following strategy.

The origins of the first and second images define their epipolar lines

$$F_{13}x + F_{23}y + F_{33}f_0 = 0, \quad F_{31}x' + F_{32}y' + F_{33}f_0 = 0 \qquad (19)$$

in the other images. If the images are fixated, the origins should be on these epipolar lines. So, the degree of fixation

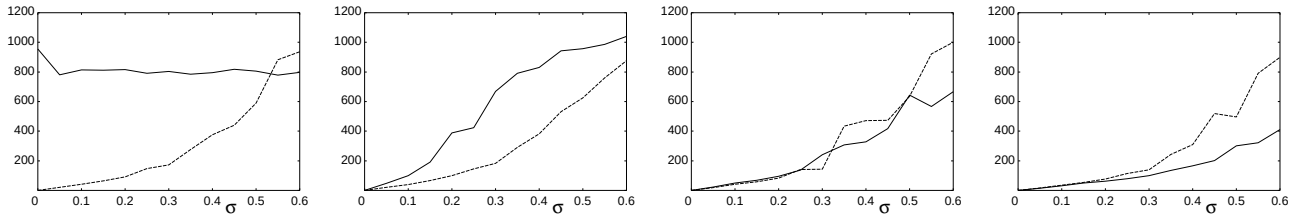

Fig. 6. The horizontal axis is for the noise standard deviation σ (pixels). The vertical axis shows the root-mean-square error in the focal lengths over 1000 trials. The solid and dashed lines are for the variable and fixed focal length methods, respectively. The value d (pixels) measures the deviation from fixation.

can be measured by the distances h and h' (pixels) of these lines from the origins, i.e.,

$$h = \frac{|F_{33}|f_0}{\sqrt{F_{13}^2 + F_{23}^2}}, \qquad h' = \frac{|F_{33}|f_0}{\sqrt{F_{31}^2 + F_{32}^2}}. \tag{20}$$

We judge that the images are fixated if $h \leq h_c$ and $h' \leq h_c$ for a threshold h_c (pixels). This judgment is independent of the scale of $\boldsymbol{F}$ or the average magnitude of the error in $\boldsymbol{F}$.

Many other switching schemes are conceivable. For example, we may conduct statistical hypothesis testing based on the covariance tensor of the computed fundamental matrix, which can be obtained as a byproduct of the renormalization computation [10, 13], or introduce model selection using the geometric AIC or the geometric MDL [8, 9, 11]. However, it is very difficult to compute these criteria precisely. If we introduce approximations or use estimates, the result is greatly influenced by the accuracy of the approximations and estimates we use. After trying many alternatives, we have concluded that the above simple criterion works the best.

In our experiments, we used the threshold h_c = 20 (pixels), partly because the relative accuracy of the variable and fixed focal length methods is reversed around d = 20 (pixels) and partly because the deviation of about 20 pixels is inevitable if humans try to take fixated images manually[4].

Fig. 7 is the simulation result using the data of Fig. 4. We incremented d from 0 (fixated images) to 30 for σ = 0.3 (pixels). The vertical axis is for the root-mean-square error E (pixels) in eq. (17). The solid and dashed lines are for the variable and fixed focal length methods, respectively; dotted line is for the hybrid method.

We can see that the hybrid method adopts the fixed focal length method when d is small and switches to the variable focal length method when d is large. The transition occurs around the value d = 20, to which the threshold for h and h' is set. As a result, the method with higher accuracy is automatically chosen irrespective of the value d.

[4]This value should be adjusted according to the image size, the image resolution, and the focal length. According to our experiments, the critical value corresponds to approximately 0.02 radians measured in the angle of view in all cases.

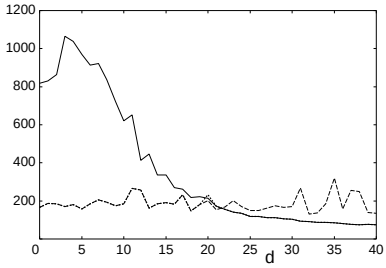

Fig. 7. The horizontal axis is for the deviation d (pixels) from fixation. The vertical axis shows the root-mean square error in the computed focal lengths for the noise standard deviation σ = 0.5 (pixels). The solid and dashed lines are for the variable and fixed focal length methods, respectively; the dotted lines are for the hybrid method.

8. REAL IMAGE EXAMPLES

In Fig. 8, the image pair (a) and (b) is fixated, while the image (c) is taken by slightly averting the optical axis. We chose 39 corresponding feature points as marked in the images. Algorithms for automatically detecting feature points and matching them are available [14], but mismatches are inevitable to some extent. Since our aim here is not to study the matching performance, we chose the feature points by hand.

We tested if the image pair (a) and (b) and the image pair (a) and (c) are fixated. The computed values of h and h' are listed in Table 1; the image pair (a) and (b) is judged to be fixated, while the image pair (a) and (c) is not.

Table 1 also lists the focal lengths f and f' computed using the two method ("variable" and "fixed" denote the variable and fixed focal length methods, respectively). According to our calibration using a reference pattern, the true focal length is $f = f' \approx 1000$ (pixels), from which the values the variable focal length method computes from the fixated image pair (a) and (b) are wide apart, while the fixed focal length method estimates a reasonable value. For the non-fixated image pair (a) and (c), both methods estimate reasonable values, but the variable focal length method gives a slightly better estimate, in agreement with the simulation results.

(a) (b) (c)

Fig. 8. Input images and selected feature points. The image pair (a) and (b) is fixated, while the image (c) is taken by slightly averting the optical axis.

Table 1. Fixation test and focal length estimation for the image pair (a) and (b) and for the image pair (a) and (c) of Fig. 8. The unit is pixels.

	fixation test		variable		fixed
	h	h'	f	f'	$f = f'$
(a), (b)	1.03	1.03	436	443	811
(a), (c)	54.22	54.22	929	906	855

9. CONCLUDING REMARKS

In this paper, we have studied the occurrences of imaginary focal lengths and the computational failure for fixated images that arise in reconstructing 3-D shape from two uncalibrated views. We have presented a remedy for these by subsampling feature points and fixing the focal length. We first summarized theoretical backgrounds and then did simulations, which revealed a rather surprising fact that when the focal length is actually fixed, not using that knowledge yields better results for non-fixated images. We proposed a hybrid method switching the computation by judging whether or not the images are fixated. Doing simulations and real image experiments, we have demonstrated the effectiveness of our method.

Acknowledgments: This work was supported in part by the Ministry of Education, Culture, Sports, Science and Technology, Japan, under a Grant in Aid for Scientific Research C(2) (No. 13680432), the Support Center for Advanced Telecommunications Technology Research, and Kayamori Foundation of Informational Science Advancement.

10. REFERENCES

[1] S. Bougnoux, From projective to Euclidean space under any practical situation, a criticism of self calibration, *Proc. 6th Int. Conf. Comput. Vision.*, January 1998, Bombay, India, pp. 790–796.

[2] M. J. Brooks, L. de Agapito, D. Q. Huynh and L. Baumela, Towards robust metric reconstruction via a dynamic uncalibrated stereo head, *Image Vision Comput.*, **16**-14 (1998), 989-1002.

[3] W. Chojnacki, M. J. Brooks, A. van den Hengel and D. Gawley, On the fitting of surfaces to data with covariances, *IEEE Trans. Patt. Anal. Mach. Intell.*, **22**-11 (2000), 1294–1303.

[4] R. I. Hartley, Estimation of relative camera position for uncalibrated cameras, *Proc. 2nd Euro. Conf. Comput. Vision*, May 1992, Santa Margherita Ligure, Italy, pp. 579–587.

[5] R. Hartley and C. Silpa-Anan, Reconstruction from two views using approximate calibration, *Proc. 5th Asian Conf. Comput. Vision*, January 2002, Melbourne, Australia, Vol. 1, pp. 338–343.

[6] R. Hartley and A. Zisserman, *Multiple View Geometry in Computer Vision*, Cambridge University Press, Cambridge, U.K., 2000.

[7] A. Heyden and K. Åström, Euclidean reconstruction from image sequences with varying and unknown focal length and principal point. *Proc. IEEE Conf. Comput. Vision Pattern Recog.*, June 1997, Puerto Rico, pp. 438–443.

[8] K. Kanatani, *Statistical Optimization for Geometric Computation: Theory and Practice*, Elsevier Science, Amsterdam, the Netherlands, 1996.

[9] K. Kanatani, Geometric information criterion for model selection, *Int. J. Comput. Vision*, **26**-3 (1998), 171–189.

[10] K. Kanatani, Optimal fundamental matrix computation: Algorithm and reliability analysis, *Proc. 6th Symp. Sensing via Image Inf.*, June, 2000, Yokohama, Japan, pp. 291–298.

[11] K. Kanatani, Model selection for geometric inference, *Proc. 5th Asian Conf. Comput. Vision*, January 2002, Melbourne, Australia, Vol. 1, pp. xxi–xxxii.

[12] K. Kanatani and C. Matsunaga, Closed-form expression for focal lengths from the fundamental matrix *Proc. 4th Asian Conf. Comput. Vision*, January 2000, Taipei, Taiwan, Vol. 1, pp. 128–133.

[13] K. Kanatani and N. Ohta, Comparing optimal three-dimensional reconstruction for finite motion and optical flow, *J. Electronic Imaging*, **12**-3 (2003-7), 478–488.

[14] Y. Kanazawa and K. Kanatani, Robust image matching under a large disparity, *Proc. 6th Asian Conf. Computer Vision*, January 2004, Jeju, Korea.

[15] Y. Leedan and P. Meer, Heteroscedastic regression in computer vision: Problems with bilinear constraint, *Int. J. Comput. Vision.*, **37**-2 (2000), 127–150.

[16] M. Pollefeys, R. Koch, R. and L. Van Gool, Self-calibration and metric reconstruction in spite of varying and unknown internal camera parameters, *Int. J. Comput. Vision*, **32**-1 (1999), 7–26.

[17] T. Ueshiba and F. Tomita, Self-calibration from two perspective views under various conditions: Closed-form solutions and degenerate configurations, *Proc. Australia-Japan Advanced Workshop on Computer Vision*, September 2003, Adelaide, Australia, pp. 118–125.

[18] Z. Zhang, R. Deriche, O. Faugeras and Q.-T. Luong, A robust technique for matching two uncalibrated images through the recovery of the unknown epipolar geometry, *Artif. Intell.*, **78** (1995), 87–119.